



MISSOURI
S&T

CENTER FOR TRANSPORTATION INFRASTRUCTURE AND SAFETY



Novel Integrated Nondestructive Testing Methodology for Detection and Evaluation of Corrosion in Cement-Based Materials

by

PI Kristen M. Donnell¹

Co-PI Mohammad Tayeb Ghasr¹

Co-PI Edward C. Kinzel²

¹Applied Microwave Nondestructive Testing Laboratory (*amntl*)

Department of Electrical and Computer Engineering

²Department of Mechanical and Aerospace Engineering
Missouri University of Science and Technology

**NUTC
R341**

**A National University Transportation Center
at Missouri University of Science and Technology**

Disclaimer

The contents of this report reflect the views of the author(s), who are responsible for the facts and the accuracy of information presented herein. This document is disseminated under the sponsorship of the Department of Transportation, University Transportation Centers Program and the Center for Transportation Infrastructure and Safety NUTC program at the Missouri University of Science and Technology, in the interest of information exchange. The U.S. Government and Center for Transportation Infrastructure and Safety assumes no liability for the contents or use thereof.

Technical Report Documentation Page

1. Report No. NUTC R340	2. Government Accession No.	3. Recipient's Catalog No.	
4. Title and Subtitle Novel Integrated Nondestructive Testing Methodology for Detection and Evaluation of Corrosion in Cement-Based Materials	5. Report Date June 2014		
	6. Performing Organization Code		
7. Author/s PI: Kristen M. Donnell Co-PI: Mohammad Tayeb Ghasr Co-PI: Edward C. Kinzel	8. Performing Organization Report No. Project #00042511		
9. Performing Organization Name and Address Center for Transportation Infrastructure and Safety/NUTC program Missouri University of Science and Technology 220 Engineering Research Lab Rolla, MO 65409	10. Work Unit No. (TRAIS)		
	11. Contract or Grant No. DTRT06-G-0014		
12. Sponsoring Organization Name and Address U.S. Department of Transportation Research and Innovative Technology Administration 1200 New Jersey Avenue, SE Washington, DC 20590	13. Type of Report and Period Covered Final		
	14. Sponsoring Agency Code		
15. Supplementary Notes			
16. Abstract The objective of this project focused on the development of a hybrid nondestructive testing and evaluation (NDT&E) methodology that combines the benefits of microwave NDT and thermography into one new technique. In this way, unique features of both NDT methods can be brought together to achieve new results that one method alone cannot achieve. Preliminary results have shown the combination of microwave and IR methods as a promising technique for detection corrosion in metals. The objective of this project is to build upon these preliminary results to investigate the feasibility of this new technique, herein referred to as Active Microwave Thermography (AMT), to detect and evaluate the presence of corrosion in cement-based materials (e.g., corrosion of reinforcing steel bars, or rebar), which is of critical importance to the nation's transportation infrastructure. Included in this investigation was the acquisition of a small AMT system (designed and built by the graduate student supported by this project) to allow investigators to perform properly controlled experiments with consideration given to incident microwave power, distribution of the microwave energy, frequency, polarization of the incident signal, etc.			
17. Key Words Cement-based materials, structural health monitoring, corrosion, reinforcing steel bars, microwave nondestructive testing, thermography, transportation infrastructure	18. Distribution Statement No restrictions. This document is available to the public through the National Technical Information Service, Springfield, Virginia 22161.		
19. Security Classification (of this report) unclassified	20. Security Classification (of this page) unclassified	21. No. Of Pages 21	22. Price

Novel Integrated Nondestructive Testing Methodology for Detection and Evaluation of Corrosion in Cement-Based Materials – Final Report

*PI Kristen M. Donnell¹, Co-PI Mohammad Tayeb Ghasr¹, Co-PI
Edward C. Kinzel²*

¹Applied Microwave Nondestructive Testing Laboratory (*amntl*)

Department of Electrical and Computer Engineering

²Department of Mechanical and Aerospace Engineering

Missouri University of Science and Technology

Submitted to:

Dr. Kamal Khayat, Director

Center for Transportation Infrastructure and Safety,
A National University Transportation Center (NUTC)
Missouri University of Science and Technology

1.0 Project Objective

The objective of this project focused on the development of a hybrid nondestructive testing and evaluation (NDT&E) methodology that combines the benefits of microwave NDT and thermography into one new technique. In this way, unique features of both NDT methods can be brought together to achieve new results that one method alone cannot achieve. Preliminary results have shown the combination of microwave and IR methods as a promising technique for detection corrosion in metals. **The objective of this project is to build upon these preliminary results to investigate the feasibility of this new technique, herein referred to as Active Microwave Thermography (AMT), to detect and evaluate the presence of corrosion in cement-based materials** (e.g., corrosion of reinforcing steel bars, or rebar), which is of critical importance to the nation's transportation infrastructure. Included in this investigation was the acquisition of a small AMT system (designed and built by the graduate student supported by this project) to allow investigators to perform properly controlled experiments with consideration given to incident microwave power, distribution of the microwave energy, frequency, polarization of the incident signal, etc.

2.0 Active Microwave Thermography

In general, thermographic NDT involves imaging/measuring the surface temperature/thermal profile of a structure or object of interest. Typically, thermography includes an active heat source to excite a thermal gradient within the structure of interest (as opposed to passively measuring/imaging the surface temperature profile). Several types of active excitation have been utilized including heat/flash lamps, as well as other non-thermal excitation methods. For example, utilizing an ultrasonic excitation in order to generate a thermal gradient has been successfully demonstrated by others. By vibrating a material via ultrasonic excitation, heat is generated at the location of flaws (defects, disbonds, etc.). Subsequently, this heat is imaged using a thermal (infrared) camera. The work investigated here suggests a similar yet unique approach through the integration of microwave methods with thermography, both established NDT techniques.

The combination of microwave NDT and thermography, herein referred to as Active Microwave Thermography (AMT), offers unique advantages and may offer a substantial improvement to traditional thermographic techniques. For example, utilizing microwave energy as a source of heat allows selective and localized heating at a location of interest (as opposed to heating an entire sample and risking possible heat damage). Further, faster inspection rates, as compared to traditional raster scanning techniques (e.g., microwave or ultrasonic imaging, etc.), may be achieved. The inspection rate of traditional thermographic techniques may also be improved, as heat transfer can be quite slow, and microwave heating is instantaneous. AMT is a relatively new hybrid method, and preliminary work has shown this method to have potential as a structural health monitoring tool [1, 2].

3.0 AMT for Detection of Corroded Rebar

Steel corrosion byproducts are electromagnetically lossy and can be easily heated using microwave energy. This property is utilized in this application of AMT, and, subsequent to microwave heating, the thermal profile of the surface of the specimen under test (SUT) is mapped using an IR camera. Utilizing microwave energy (as opposed to other heat sources) is advantageous since microwave energy can penetrate concrete and locally heat the area of interest.

In order to study the interaction between an electromagnetic signal and induced heating, a coupled microwave and thermal simulation model was constructed using the CST MICROWAVE STUDIO[®] and MPHYSICS STUDIO[®] [3]. This model allowed the electromagnetic (specifically, polarization of the incident signal) and thermal properties exhibited by corroded rebar surrounded by air under planewave incidence to be studied. First, the thermal response resulting from microwave heating was simulated for an infinitely-long rebar as a function of (uniform) corrosion thickness. A second simulation was conducted to study the electromagnetic and thermal properties of a finite-length rebar with an area of corrosion. Lastly, a third CST simulation was developed that examined the thermal response of two finite lengths of rebar, one fully corroded and one clean (i.e., without corrosion), embedded in a concrete block. In all cases, a frequency of 2.45 GHz (in the ISM band) was selected for the incident microwave energy. This frequency was selected due to previous success with frequencies in the range for cement-based materials characterization.

3.1 Simulation of Rebar in Air

To begin studying the relationship between microwave heating and corrosion, an infinitely-long rebar of radius 4.8 mm with uniform corrosion on its surface was simulated under steady-state illumination conditions (meaning the rebar was under continuous electromagnetic illumination). While an infinitely-long rebar will not be found in practice, studying such an element removes effects that may result from the geometry (i.e., finite rebar length) of a more practical model. For this model, the corrosion replaced part of the volume of the rebar (so as to properly reflect the corrosion process), meaning the radius of the steel core of the corroded rebar decreased as corrosion thickness increased. Specifically, the radius of the rebar decreased by 50% of the corrosion thickness. The rebar was assumed to be made of steel (AISI 1008). The corrosion had a relative permittivity, $\epsilon_r = 10$ and loss tangent, $\tan \delta = 0.2$ (a typical value for steel corrosion [4]), thermal conductivity, $k_t = 0.6$ W/m·K, specific heat, $c_p = 650.6$ J/kg·K, and density $\rho = 5242$ kg/m³ [5, 6]. The background material was assumed to be air ($\epsilon_r = 1$, electrical conductivity, $\sigma = 0$ S/m, $k_t = 0.024$ W/m·K, $c_p = 1005$ J/kg·K, and $\rho = 1.293$ kg/m³). The magnitude of the incident electric field of the planewave was chosen to be 2500 V/m, in order to simulate a 50 W microwave source radiating from an R-band (1.7 – 2.6 GHz) waveguide aperture. This value was calculated using Eq. (1), below, where E_0 is incident electric field strength, η is the impedance of the material in which the planewave is propagating (377 Ω for free-space), P is the total power, and A is the aperture of the radiating antenna (i.e. cross-section of the waveguide).

$$E_0 = \left(2\eta \frac{P}{A} \right)^{1/2} \quad (1)$$

Using the model for an infinitely-long rebar, the effect of polarization on the thermal response of the rebar was investigated as a function of corrosion thickness. To this end, signals with polarization orthogonal and parallel to the length of the rebar were considered. In addition, the response from a circularly-polarization signal was also studied. From these (steady-state) excitations, the resultant (electromagnetically-induced) thermal losses and subsequent maximum temperature increase of the rebar were calculated. The maximum temperature difference (as compared to the initial/ambient temperature of the rebar) for the three different polarizations as a function of corrosion thickness can be found below in Fig. 1.

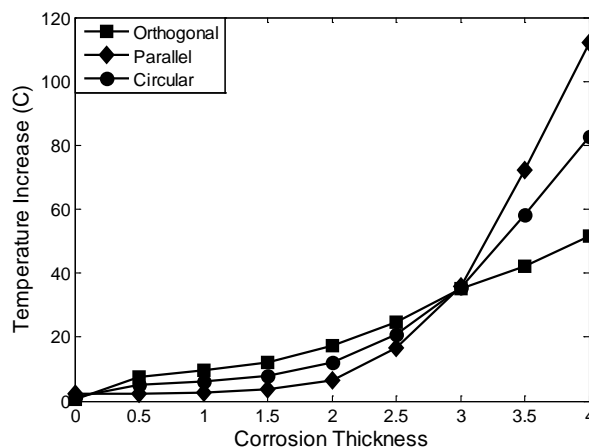


Fig. 1: Maximum temperature of corroded rebar for different polarizations as a function of corrosion thickness.

As mentioned above, corrosion by-products are electromagnetically lossy. As such, it is expected that as the thickness of corrosion increases, so should the microwave-induced heating. This behavior is evident in Fig. 1 for all three polarizations. It can also be seen that as the thickness of corrosion increases, the temperature increase due to the parallel-polarized signal follows an exponential curve, while the effect of orthogonal polarization is linear. Furthermore, for corrosion of less than 3 mm, orthogonal polarization is optimal, while for significant corrosion (> 3 mm), parallel becomes best. This is important since, depending on the severity of corrosion, the polarization can be optimized to achieve maximum heating (if the orientation of the rebar is known). It can also be seen that the induced heat from circular polarization is the average of the heating from parallel and perpendicular polarization. While circular polarization does not result in the maximum induced heat, it does offer an independence from a-priori knowledge of rebar orientation (with respect to the polarization of the incident signal), as well as an independence with respect to corrosion thickness. This is important since knowledge of the orientation of the rebar may not be available in practice. However, utilizing circular polarization will be at the expense of a more sophisticated microwave antenna and/or measurement system.

Once the effect of polarization was understood, a finite-length rebar (in this case, 10 cm), a portion of which is corroded, was simulated, as is shown below in Fig. 2a. In this case, a 0.1 mm layer of corrosion was considered (length of the corroded section is 2 cm). The material properties for the steel rebar and corrosion remain as above. In this case, the magnitude of the incident electric field was chosen to be 500 V/m (calculated using Eq. (1)), in order to simulate a

10 W source incident on an area of $17\text{ cm} \times 15\text{ cm}$ (a relatively small footprint for inspection, utilizing fairly low power). All three polarizations were considered with the results shown below in Fig. 2b-d.

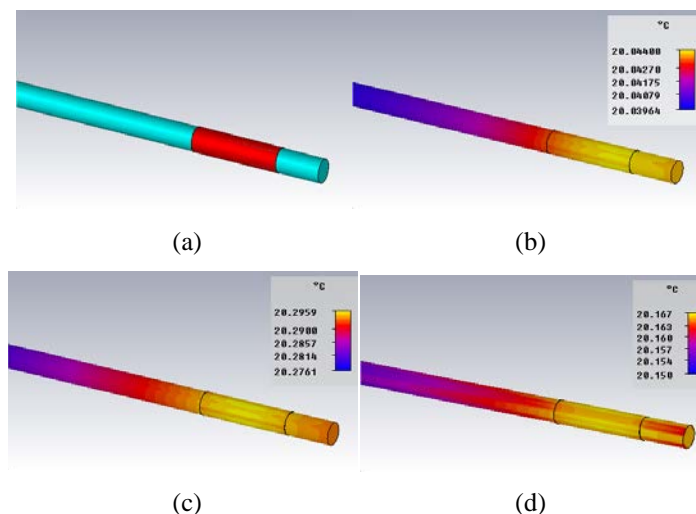


Fig. 2: (a) Simulated rebar with corroded section. Heat distribution caused by (b) orthogonal polarization, (c) parallel polarization, and (d) circular polarization.

Fig. 2 shows that, in this case, the polarization of the incident signal does not affect the heat distribution on the rebar. However, as in case of the infinitely-long rebar, more significant heating was evident in the corroded region as compared to the non-corroded region of the rebar. Furthermore, parallel polarization was found to cause the most heating, providing a temperature increase of 20° mC . The temperature increase for circular polarization was 17° mC , and for orthogonal polarization, 5° mC . While the increase in temperature simulated here is fairly small, this is not of concern, as the incident power considered is quite low (10 W), and the sensitivity of modern IR cameras is on the order of 50° mC or less. As such, with a reasonable increase in incident power, the change in temperature would be within a detectable range.

It is important to note that these results differ from those in Fig. 1, as according to Fig. 1, orthogonal polarization is best for thin corrosion. The results of Fig. 1 are for a completely-corroded infinitely-long rebar (allowing for a study of the sole effect of polarization), whereas Fig. 2 highlights results of a partially-corroded finite-length rebar where the geometry of the rebar (e.g., finite length/edge effects) may affect the results.

3.2 Simulation of Rebar Embedded in Concrete

In order to investigate a more practical scenario, a simulation was conducted to model an embedded case. More specifically, two steel (AISI 1008) rebar sections (each of length 15 cm and radius 4.8 mm), one fully corroded and one uncorroded, were embedded (parallel to one another) in a concrete block ($17\text{ cm} \times 15\text{ cm} \times 5\text{ cm}$). The rebars were placed a distance of $\sim 4\text{ cm}$ apart. The rebars were located $\sim 1.6\text{ cm}$ from the bottom of the block, and $\sim 3\text{ cm}$ from the top.

The corrosion was assumed to have the same electromagnetic and thermal properties as provided above. The concrete was assumed to have $\epsilon_r = 5$, $k_t = 1.73 \text{ W/m}\cdot\text{K}$, $c_p = 800 \text{ J/kg}\cdot\text{K}$, and $\rho = 2400 \text{ kg/m}^3$. A 10 W electromagnetic source operating at 2.45 GHz was assumed (as above).

To begin, the effect of polarization was studied. The CST model and heat distribution of the shallow side of the block for orthogonal, parallel, and circular polarization are shown in Fig. 3. The corroded bar (corrosion thickness 1 mm) is on the left. It can be observed that although parallel polarization (14° mC , Fig. 3c) creates less heating than orthogonal polarization (25° mC , Fig. 3b), the heat generated is more uniform along the length of the surface above the corroded rebar. Additionally, the temperature increase generated by circular polarization (19° mC , Fig. 3d) is approximately the average of parallel and perpendicular polarizations and also exhibits slightly less uniform heating over the length of the rebar. It is interesting to note that the results of Fig. 3 corroborate those of Fig. 1. Since the embedded concrete model considers a fully-corroded rebar, it is more similar to the infinitely-long model discussed above. As such, it is not unexpected that the results shown here may be similar to those of Fig. 1.

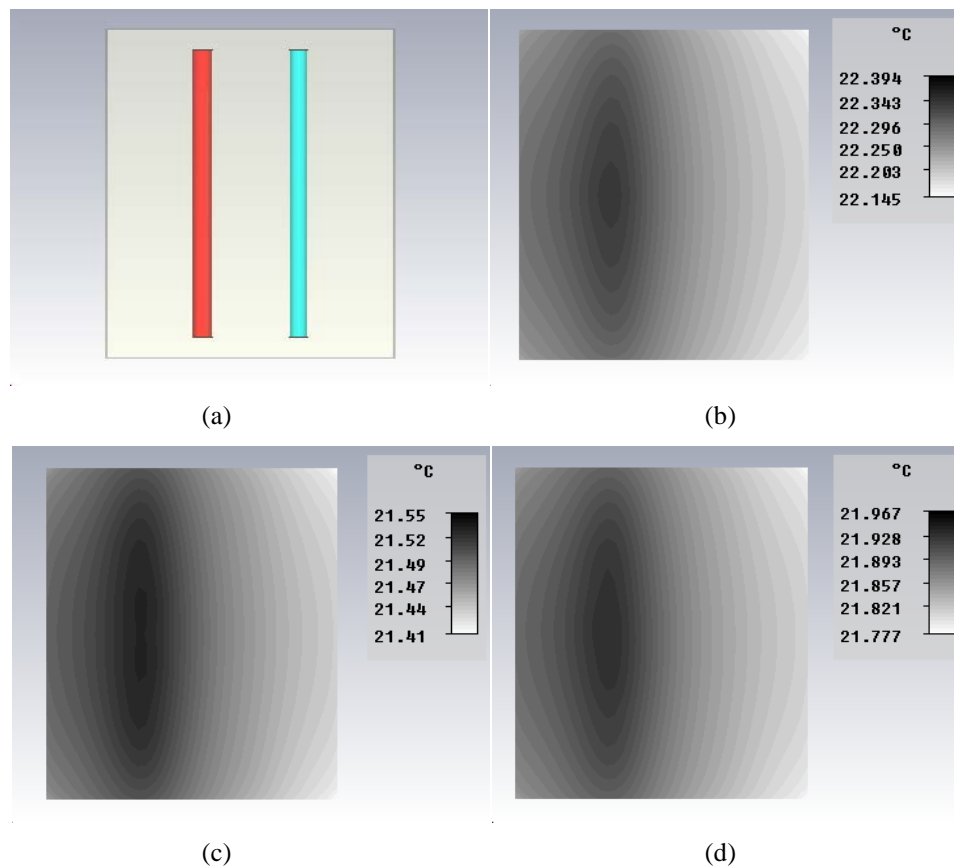


Fig. 3: (a) Corroded (left) and non-corroded (right) rebar samples embedded in shallow (1.6 cm) concrete. Heat distribution caused by (b) orthogonal polarization, (c) parallel polarization, and (d) circular polarization.

Next, simulations were conducted to investigate the effect of the loss tangent of the concrete on the induced heat. In practice, a concrete structure may be subject to moisture ingress, which

would affect the electromagnetic properties of the concrete resulting in an increase in loss tangent. As the loss tangent of the surrounding material increases, more of the microwave energy may be absorbed in this material, resulting in more heating of the surrounding material and less energy impinging upon the corrosion thus less induced heating of the corrosion. For this simulation, orthogonal polarization was assumed (shown in Fig. 1 to be optimal for thin corrosion), with a corrosion thickness of 1 mm. Fig. 4a shows the temperature difference, as a function of loss tangent of concrete, between the maximum temperature on the surface of the concrete block located above the corroded rebar with respect to the temperature above the clean rebar. Upon considering these results, a few important points can be made. First, for low moisture conditions (represented above by a loss tangent of $\sim 0.1 - 0.3$), as the loss tangent increases, a decrease in temperature difference is evident. This indicates that even though the concrete absorbs more of the microwave energy, the presence of corrosion is still evident. However, for conditions of increased moisture presence (represented here by a loss tangent of 0.3 or greater) the temperature above the rebar exhibits very little change. This may be limiting with regards to detection of corroded rebar, but points to another potential application of this method, namely, detection of moisture ingress. The temperature sensitivity to the presence of corrosion may be improved by increasing the incident power (as only 10 W was considered here) or utilizing circular polarization.

Finally, simulations were conducted to investigate the effect of corrosion thickness on heating, with a fixed concrete loss tangent of 0.1. The maximum temperature on the surface of the concrete block (above the corroded rebar) as a function of corrosion thickness is shown in Fig. 4b. In this case and as expected, the temperature increases proportionally to corrosion thickness.

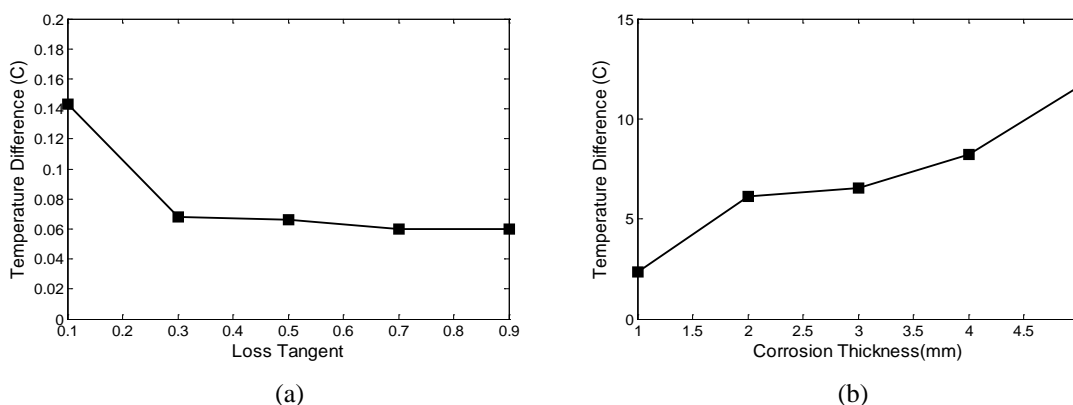


Fig. 4: Maximum surface temperature as a function of (a) loss tangent of concrete, and (b) corrosion thickness.

A last simulation was conducted to investigate the potential of this method to detect corroded rebar under thick (3", 7.6 cm) concrete cover. Simulation conditions remained as above (see Fig. 3), with a 100 W, circularly-polarized, incident signal assumed. The CST model and surface thermal profile are shown in Fig. 5. In this case as well, the presence of a corroded rebar is evident in the surface thermal profile. This is quite important as it relates to the potential of AMT for detection of corroded rebar, as the concrete cover may differ from case to case. However,

high power requirements may limit the use of AMT for inspecting rebars under thick concrete cover.

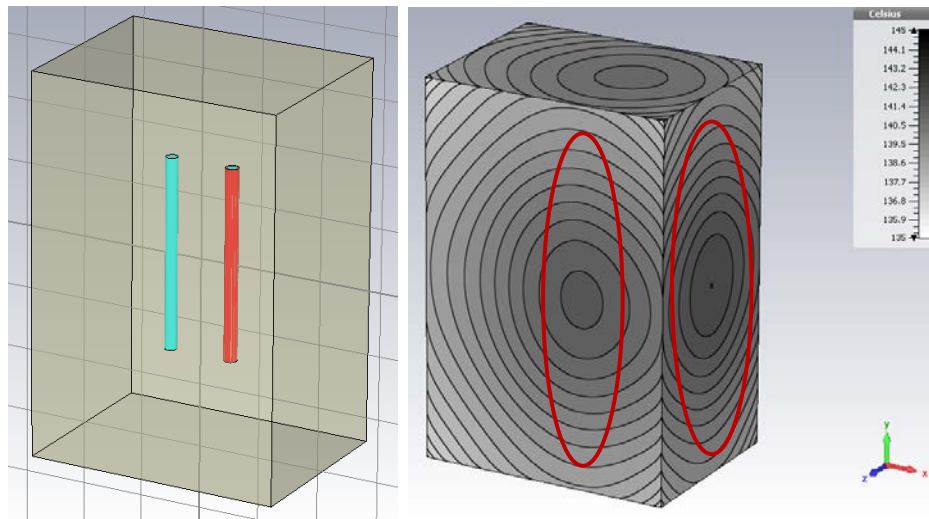


Fig. 5: Thermal profile for rebar with thick concrete cover.

Overall, the simulations presented above indicate AMT has significant potential as a nondestructive testing tool for the infrastructure industry. To this end and to lend further credence to this new proposed technique, measurements were conducted on clean and corroded rebar in air and embedded in a concrete block. For these preliminary proof-of-concept measurements, a commercial countertop microwave oven (the only available high power source at the time) was used as the source of the microwave energy (the only available high power source at the time). As such, direct comparison to the simulated results above is not possible, as the signal within a microwave oven is significantly different than the incident signal (planewave) considered above.

3.3 Rebar in Air

To begin, two rebar samples were obtained; one with light corrosion (on the order 0.2 mm or less) along half of its length, the other with localized significant corrosion (on the order of 1-4 mm) on a portion of its length. These rebar samples are shown below in Fig. 6a. Each of these samples was exposed to microwave energy for 5 sec, and immediately following, imaged using a thermal camera (FLIR Thermacam SC 500), shown below in Fig. 6b-c (corroded area indicated in the black oval). It should be noted that the samples were placed on a plastic platform for testing, which is evident in the images below.

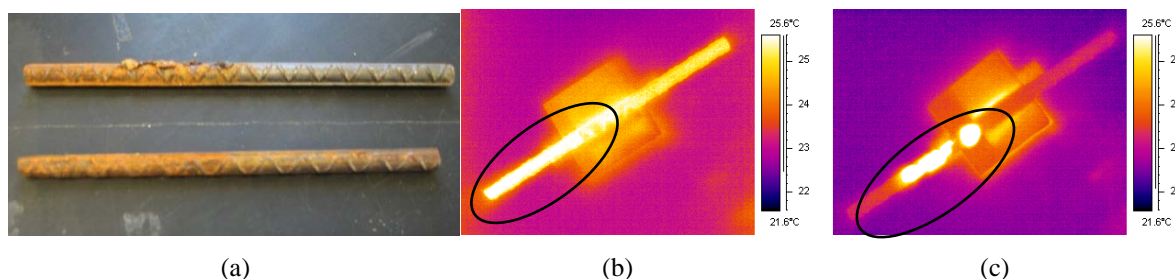


Fig. 6: (a) Rebar with localized significant (top), and light corrosion (bottom). Thermal image of rebar with (b) light corrosion, and (c) localized corrosion.

As can be seen in Fig. 6b-c, for both light and significant corrosion, the corrosion exhibited increased heating as opposed to the clean rebar. For the case of the lightly-corroded rebar, the temperature increase was nearly 600° mC (well above the sensitivity of the FLIR thermal camera, 100° mC). In addition and as expected, more heat was generated in the localized significant corrosion (nearly 3000° mC), as compared to the light corrosion. While these results are quite encouraging, it is also important to more accurately replicate what may be found in practice. To this end, a concrete sample with clean and corroded rebar was cast, and measurements were performed using this sample as well.

3.4 Rebar Embedded in Cement

As shown below in Fig. 7, a concrete sample (dimensions of $17\text{ cm} \times 15\text{ cm} \times 5\text{ cm}$) containing two rebars (one clean and one highly corroded) was cast using Quikcrete™ brand concrete mix. The rebars were embedded $\sim 2.5\text{ cm}$ in the concrete. After 24 hours, the sample was demolded and placed in an oven (for ~ 1 week) at a temperature of 38°C to remove additional water in the sample. After removing the sample from the oven and allowing it to return to ambient temperature, the sample was exposed to 15 sec of microwave energy. Then, using the same thermal camera as above, an image was captured of the sample (see Fig. 7). Clearly (and as indicated by the black oval), the corroded rebar is detectable in the thermal image after microwave heating. The clean rebar is also evident in the image as well (left of the black oval), appearing as a lower-temperature line. Uneven heating is also evident in the sample, potentially due to the distribution of the microwave energy in the commercial microwave oven.

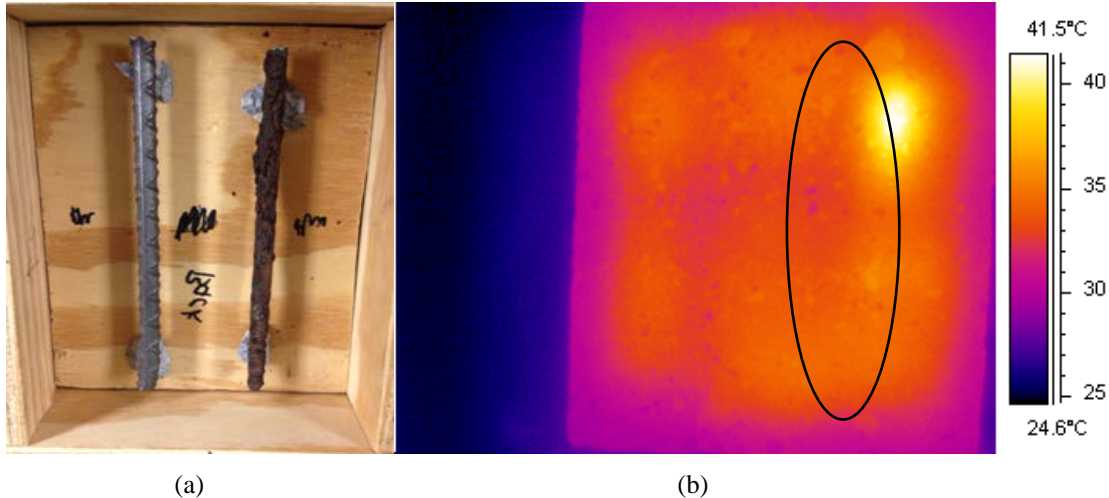


Fig. 7: Photograph of clean (left) and corroded (right) rebar, and (b) thermal image of concrete block surface after microwave heating (location of corroded rebar indicated in the black oval).

The preliminary results presented above clearly indicate that AMT has strong potential as an NDT tool for the transportation and infrastructure industries. The presence of corroded rebar has been shown to be detectable using this hybrid NDT technique. To further investigate the potential of AMT for structural health monitoring in the infrastructure, another aspect of structural health monitoring, namely, detection of disbonds in rehabilitated cement-based structures, was investigated. The preliminary findings of this additional (to the original project objective) investigation are presented next.

4.0 AMT for Disbond Detection

One method for rehabilitation of cement-based (e.g., concrete) structures is through the application of glass- or carbon-based fiber reinforced polymer (FRP) composite materials to the structure surface. Evaluation of such structures is important since the structural performance of these structures is usually limited by the FRP-concrete interface bond quality. Thus, detection of regions where the FRP has debonded from the concrete is of critical importance in order to assure the integrity of the rehabilitated/repared structure throughout its service life. In addition to normal service loading, structures that have been rehabilitated with FRP composites are also subject to environmental degradation as well as other types of damage, emphasizing the need for methods capable of detecting various types of flaws (i.e., disbonds, delaminations, voids, etc.) in such structures.

When using AMT, in general there are two mechanisms by which heat may be generated. First, (direct) dielectric heating may take place (related to the loss factor of the SUT and the heat mechanism utilized above for detection of corroded rebar). If a defect is present, it may affect the generation of heat and/or the diffusion of heat to the surface of the SUT (where the thermal camera captures the temperature profile). Another possibility may occur if conductive materials are present in the SUT (as is the case with carbon-based FRP). Microwaves cannot penetrate through conductive materials, but current will be induced in such materials when irradiated by

microwave energy. Thus, these currents may also act as a (secondary) source of heat, and the presence of a defect may again affect the resultant heat diffusion. In the case of rehabilitated cement-based structures, (conductive) carbon-based (CFRP) composites are often used for such rehabilitations [7]. As CFRP is electrically conductive, current is induced in the CFRP when irradiated by microwave energy. Thus, the presence of a defect (i.e. debonded portion of the CFRP) will affect the diffusion of heat through the structure, and may be evident in the surface temperature profile. In order to investigate the potential of AMT for inspection of such structures, preliminary simulations and measurements were conducted. In particular, the effect of incident power and disbond dimensions on the ability to detect the presence of a disbond is investigated through simulations, along with preliminary AMT measurements on a mortar specimen covered by a carbon fiber patch containing a debonded area.

4.1 Simulations - Disbond Detection

To investigate the potential of AMT for inspection of rehabilitated structures, a small concrete sample with dimensions of $30 \times 30 \times 5 \text{ cm}^3$, partially covered by a CFRP sheet, is considered. The CFRP sheet has dimensions of $20 \times 20 \times 0.2 \text{ cm}^3$, and contains a disbond (cross sectional area of $4 \times 4 \text{ cm}^2$ and depth of 2 mm), with a center offset point of 3 cm with respect to the center point of the SUT in both the x- and y- directions. The geometry of the structure is illustrated in Fig. 8.

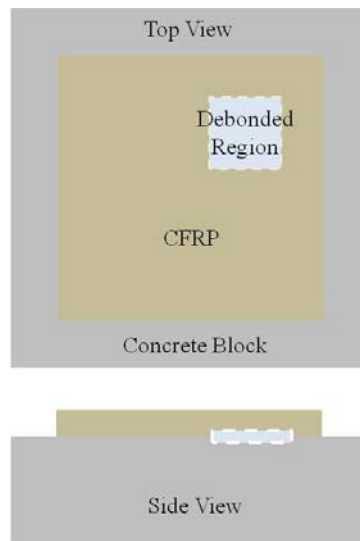


Fig. 8: Top and side views of the SUT covered by CFRP.

For this structure (under microwave illumination), the AMT-induced current in the CFRP will act as a heat source, adding to any dielectric heating that may occur resulting from the dielectric properties of the concrete itself. The relative dielectric properties, ϵ_r , of the concrete (SUT) are assumed to be $\epsilon_r = 10 - j4$ [8].

A coupled microwave-thermal simulation was conducted using CST Microwave Studio[®] and MPHYSICS Studio[®] for this structure [3]. The simulation is completed in two parts; first, the electromagnetic response (i.e., induced currents, etc.) of the SUT under planewave illumination

is determined. Then, based on the electromagnetic response, the thermal response (i.e., heat generation and diffusion, etc.) of the structure is calculated. Temporally, the simulation is described first by the amount of time the SUT is illuminated by microwave energy (i.e., the heating time), t_1 , and subsequently by the amount of time the thermal profile on the surface of the SUT is measured (i.e., the cooling time), t_2 .

As above (for the investigation involving corroded rebar), the magnitude of the incident electric field was related to an incident power level through Eq. (1). In all cases, a frequency of 2.45 GHz was used and assumed to be radiating from a standard R-band (1.7-2.6 GHz) waveguide (aperture of $109.22 \times 54.61 \text{ mm}^2$). Concrete was assumed to have a thermal conductivity of $k_t = 1.7 \text{ W/m.K}$, specific heat of $c_p = 0.8 \text{ kJ/kg.K}$, and density of $\rho = 2400 \text{ kg/m}^3$, air was assumed to have $k_t = 0.026 \text{ W/m.K}$, $c_p = 1.005 \text{ kJ/kg.K}$, and $\rho = 1.204 \text{ kg/m}^3$, and CFRP was assumed to have $k_t = 200 \text{ W/m.K}$, $c_p = 0.71 \text{ kJ/kg.K}$, and $\rho = 2200 \text{ kg/m}^3$ [3, 10]. As can be seen from these properties, the thermal conductivity of concrete is much higher than air. This is important for this application of AMT, since it is expected that during the heating time, the debonded area will have a higher temperature than the remaining area of the CFRP sheet (resulting from the lower thermal conductivity of air). Thus, the disbond will appear as a hot spot on the thermal surface profile.

To begin, the effect of incident power on the thermal response of the SUT was investigated. Specifically, power levels of 30, 90 and 150 W were considered. For these simulations, an excitation time, t_1 , of 5 seconds was assumed. The normalized (with respect to ambient) temperature distributions on the surface of the CFRP (surrounding concrete not shown) for these power levels are shown below in Fig. 9 (at $t = t_1^+$, immediately after microwave illumination has ended). These results are provided for different levels of temperature sensitivity (scales of 5, 10, and 50 mK) to illustrate two important points: first, what is theoretically possible using AMT for this application, and second, the (practical) effect of thermal camera sensitivity on the technique.

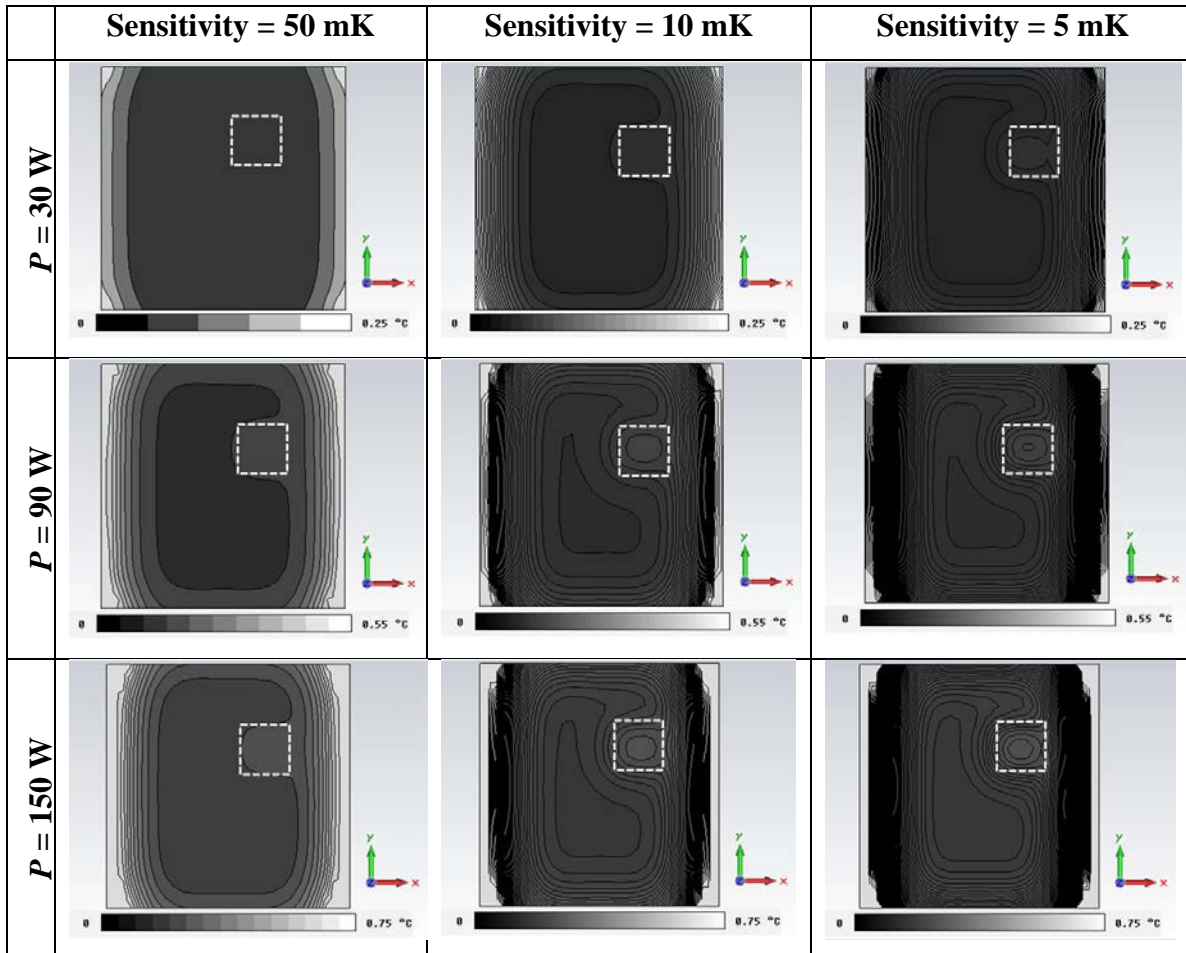


Fig. 9: Temperature distribution of the CFRP (surrounding concrete not shown) for different incident power levels and thermal sensitivities (location of disbond is indicated by the white dashed line).

The results of Fig. 9 illustrate a few practical points. First, as expected, lower incident power levels will require a more sensitive thermal camera to detect the presence of a disbond. This is evident in the results considering a 30 W source (top row of Fig. 9). More specifically, with a sensitivity of 50 mK (a typical thermal camera sensitivity, top left in Fig. 9), the disbond is not detected. However, as the resolution of the image is improved (simulating the effect of using a more sensitive thermal camera), the disbond becomes evident through the non-uniform surface temperature distribution. This is important as it illustrates potential of AMT, albeit requiring more advanced thermal detection (that may or may not be currently commercially available or cost-effective). Conversely, as the power is increased for a given measurement sensitivity (for example, 50 mK, left column of Fig. 9), the presence of the disbond becomes obvious. In fact, given a sensitivity of 50 mK, it can be seen that the ability to detect the disbond (from the thermal profile), is effectively not improved by increasing the incident power from 90 W to 150 W, indicating that the required power may be optimized per different applications. Further, these results also indicate that it may be more straightforward to quantify the dimensions of a disbond using a lower power level (rather than one that results in a more detailed thermal profile). This is quite important practically as it relates to the minimum energy required for successful detection

and quantification while minimizing the risk of thermal damage. Lastly, it is also evident that the most significant temperature increase is located at the edges of the CFRP. This occurs due to the polarization of the incident energy (here, the polarization was linear and in the x-direction, with respect to the coordinates shown in Fig. 9). Thus, the currents induced in the CFRP will also flow in the x-direction. Consequently and based on edge effects [11], the induced current density is most dense at the edges, resulting in the most significant temperature increase. This effect is increasingly obvious as the incident power is increased (bottom row of Fig. 9).

In order to study the effect of disbond size on the temperature distribution, different cross-sectional areas of the disbond were considered, and the resulting change in temperature at the top surface of the CFRP analyzed. For these simulations, an incident power level of 50 W was assumed (selected as a relatively low power that may still provide enough energy for practical detection), with the same heating time as above. The results are shown immediately after microwave illumination has ended (i.e., $t = t_I^+$). The surface temperature profile for 4 different cross-sectional areas, 2×2 to 5×5 cm², is shown in Fig. 10. A temperature sensitivity of 10 mK is assumed for all cases.

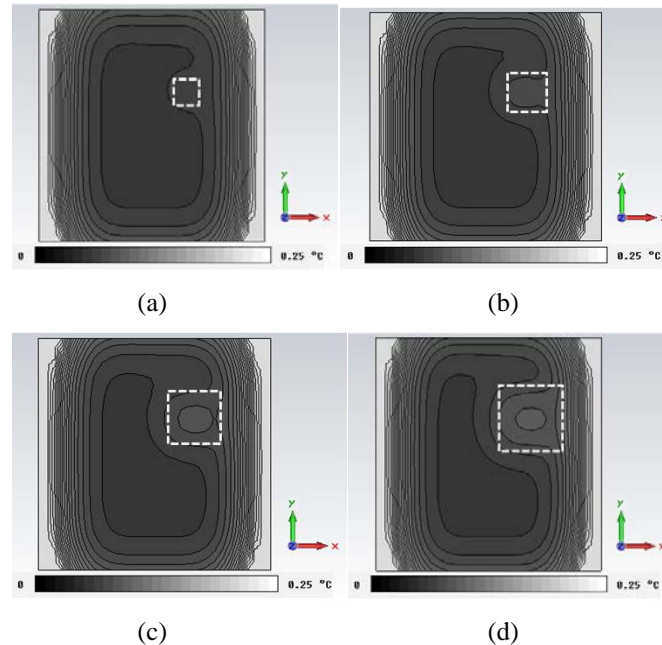


Fig. 10: Surface temperature distribution with incident power of 50 W for disbond dimensions of (a) 2, (b) 3, (c) 4, and (d) 5 cm² (location of disbond is indicated by the white dashed line).

As shown in Fig. 10, the dimensions of the disbond clearly have an effect on the surface temperature distribution. For example, in Fig. 10a (2 cm^2 disbond), the temperature distribution is just beginning to provide an indication of the presence of the disbond. This indication becomes increasingly stronger as the disbond dimensions increase, as shown in Fig. 10c-d. It should be noted that while the assumed thermal sensitivity is quite high (10 mK) and consequently may be difficult to achieve with reasonably-priced (commercially-available) thermal cameras, this practical limitation may be alleviated by increasing the incident power (i.e., similar to what is

shown above in Fig. 9). More expensive (externally-cooled) commercially-available thermal cameras may also offer the sensitivity required for low incident power.

Further, the inclusion of more advanced measurement and signal processing techniques (taking advantage of the legacy of thermography) may also improve the ability to detect such disbonds using lower power levels along with a typical thermal camera (sensitivity on the order of 50 mK) [12].

4.2 Disbond Detection Measurements

To further investigate the feasibility of AMT for inspection of rehabilitated cement-based structures, preliminary measurements have been performed using an AMT system (a project objective and direct result of this grant, designed and built by the graduate student involved in this investigation) that is capable of transmitting 50 W and operates at 2.4 GHz. The high power microwave energy is generated using an HP8690B Sweep Oscillator and an OphirRF 5303084 power amplifier. A horn antenna is used to illuminate the sample with this microwave energy. A DRS Tamarisk 320 thermal camera [13] with a sensitivity of 50 mK was used to measure the thermal profile on the surface of the SUT. The SUT was a mortar sample with dimensions of $20 \times 20 \times 4$ cm³ covered with a 13×13 cm² CFRP (attached using adhesive), similar to the simulated SUT shown above in Fig. 8. A disbond was created (through a lack of adhesive) with dimensions of 2×2 cm², located offset from the center of the sample. The measurement setup and mortar sample is shown in Fig. 11 (the location of the disbond is indicated by the white dashed line in Fig. 11c).

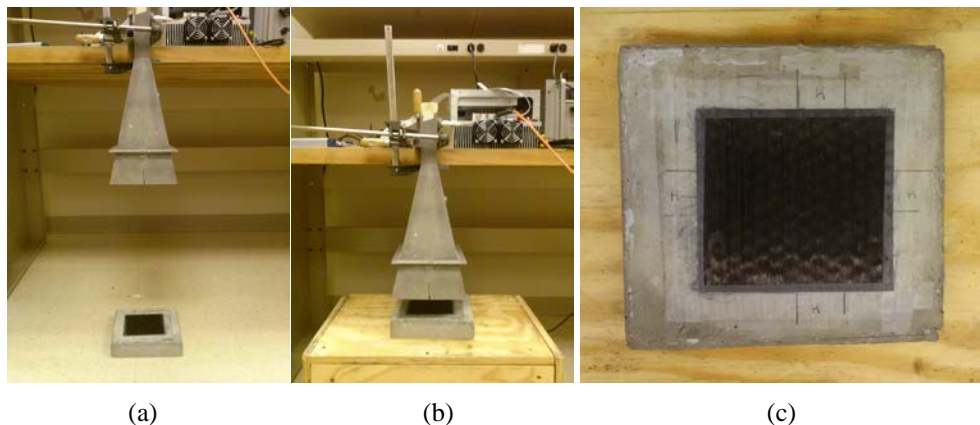


Fig. 11: AMT measurement system used for for (a) 45 cm and (b) 6 cm standoff, (c) photograph of mortar sample with disbond.

Measurements were made on the mortar sample using the AMT system at standoff distances (distance between the horn aperture and SUT) of 6 cm (Fig. 11b) with a corresponding 5 sec heating time, and 45 cm (Fig. 11c) with a corresponding 15 sec heating time. Thermal images were obtained before and after heating, as shown in Fig. 12.

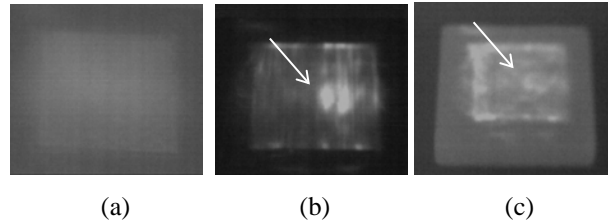


Fig. 12: Measurements on mortar sample (a) before heating, (b) 6 cm standoff, after 5 sec heat, (c) 45 cm standoff, after 15 sec heat.

As can be seen, the presence of the disbond is clear, even after heat duration of only 5 sec (Fig. 12b). This is quite significant as it relates to practical issues such as heat damage to a structure, as the incident power and heating time were quite low. In addition (and similar to the results of Fig. 9 - Fig. 10), edge effects are also evident (Fig. 12c-d). It is also interesting to note that the surface of SUT, covered by CFRP, is evident in the thermal image before the concrete sample was exposed to microwave energy (Fig. 12a). This may be a result of differences in thermal properties (reflectivity) of carbon fiber and concrete. On the other hand, the disbond is not visible prior to microwave heating. It should also be noted that while the sample was made of mortar (as opposed to concrete), the same results would be obtained had the sample been made of concrete, since the heating mechanism in this case is the induced current within the CFRP (not related to the dielectric material on which the CFRP is bonded).

5.0 Concluding Remarks

Overall, the results of this preliminary investigation indicate that AMT is a promising new inspection method for the infrastructure and transportation industries. Two potential applications of AMT have been investigated; namely, detection of corroded rebar and evaluation of rehabilitated cement-based structures.

5.1 Future Work

As AMT is a relatively new NDT technique with very little application to structural health monitoring thus far, there are many aspects that can be further investigated. Included within the plans of the PI for future work is a more controlled study on detection of corroded rebar, now that a functioning AMT system is available, as well as a study on the optimization of power levels, polarization and frequency of the incident microwave energy. Also included in this study will be different types of concrete and varying rebar coverage depths. The subsequent understanding gained here may also open the door for other (related) AMT applications such as detection of cracks in metals or corrosion under paint.

Related to this, additional investigations are planned focusing on inspection of composite structures (including further investigation into inspection of rehabilitated cement-based structures). This may include investigating the application of AMT to all-composite (carbon and/or glass-based) structures, as well as a feasibility study into the application of AMT to all

carbon-based composite structures (structures that traditional microwave NDT is unable to inspect for subsurface defects).

5.2 Project Deliverables

The project deliverables (outside of the Final Report) for this award focused on publications (specifically, submission of a journal paper to a suitable, peer-reviewed journal). Below are the publications and presentations that have resulted from the research supported by this award thus far. Additional publications will result after submission of the final report.

Related to this, two proposals have been submitted as a result of this Grant (one to the National Science Foundation and one to the United States Air Force). An additional proposal (for submission to the National Science Foundation) related to this work is under preparation at the time of this report preparation.

5.3 Publications and Student Support

The following publications and presentations have resulted from this Grant:

1. Foudazi, A., M.T. Ghasr, and K.M. Donnell, "Application of Active Microwave Thermography to Delamination Detection", *Proceedings of the International Instrumentation and Measurement Technology Conference*, pp. 1567-1571, May 12-15, 2014, Montevideo, Uruguay.
2. Foudazi, A., M. Fallahpour, and K.M. Donnell, "Effect of Material Properties on Active Microwave Thermography", *Presented at the ASNT 23rd Research Symposium*, March 24-27, 2014, Minneapolis, MN.
3. Foudazi, A., M. Fallahpour, and K.M. Donnell, "Green's Function for Evaluation of Microwave Power used for Active Microwave Thermography", *Presented at the ASNT 23rd Research Symposium*, March 24-27, 2014, Minneapolis, MN.
4. Pieper, D., K.M. Donnell, M.T. Ghasr, and E.C. Kinzel. "Integration of Microwave and Thermographic NDT Methods for Corrosion Detection" *Proceedings of the 40th Annual Review of Progress in Quantitative Nondestructive Evaluation Conference, American Institute of Physics, Conference Proceedings 1581*, pp. 1560-1567. AIP Publishing, 2014.

PI Donnell was also invited to present this work at MoDOT in Jan. 2014.

1. Donnell, K.M., Invited Presentation, Missouri Department of Transportation (MoDOT), "Active Microwave Thermography (AMT) for Inspection of Cement-Based Structures", Jan. 2014, Jefferson City, MO.

Additionally, the following students have been supported on this Grant:

1. Mr. Ali Foudazi, PhD EE student, Applied Microwave Nondestructive Testing Laboratory (*amntl*), Department of Electrical and Computer Engineering, Missouri University of Science and Technology
2. Mr. Dustin Pieper, MSEE student, Applied Microwave Nondestructive Testing Laboratory (*amntl*), Department of Electrical and Computer Engineering, Missouri University of Science and Technology

3. Mr. Sanjay Tadepally, MSEE student, Applied Microwave Nondestructive Testing Laboratory (*amntl*), Department of Electrical and Computer Engineering, Missouri University of Science and Technology

6.0 References

1. D. Pieper, K. M. Donnell, M. T. Ghasr, and E. C. Kinzel, "Integration of Microwave and Thermographic NDT Methods for Corrosion Detection", *40th Annual Review of Progress in Quantitative Nondestructive Evaluation Conference, Baltimore, MD*, July 21-26, 2013.
2. Foudazi, A., M.T. Ghasr, and K.M. Donnell, "Application of Active Microwave Thermography to Delamination Detection", *Proceedings of the International Instrumentation and Measurement Technology Conference*, pp. 1567-1571, May 12-15, 2014, Montevideo, Uruguay.
3. CST - Computer Simulation Technology, <http://www.cst.com>, accessed Feb. 2014.
4. Qaddoumi, N., L. Handjojo, T. Bigelow, J. Easter, A. Bray and R. Zoughi, "Microwave Corrosion Detection Using Open-Ended Rectangular Waveguide Sensors," *Materials Evaluation*, vol. 58, no. 2, 178-184, February 2000.
5. Laaidi, N., Belattar, S., Elbaloutti, A., "Thermal and Thermographical Modeling of the Rust Effect in Oil Conduits", *10th European Conference on Non-Destructive Testing*, June 2010
6. http://www.wolframalpha.com/input/?i=iron%28III%29+oxide&lk=1&a=ClashPrefs_*Chemical.IronIIIoxide - (accessed 8/26/13).
7. S. Kharkovsky, A. C. Ryley, V. Stephen, and R. Zoughi, "Dual-polarized near-field microwave reflectometer for noninvasive inspection of carbon fiber reinforced polymer-strengthened structures", *IEEE Trans. on Instrumentation and Measurement*, vol. 57, no. 1, pp. 168-175, January 2008.
8. S. Peer, Case, J.T.; Gallaher, E.; Kurtis, K.E.; Zoughi, R., "Microwave reflection and dielectric properties of mortar subjected to compression force and cyclically exposed to water and sodium chloride solution," *IEEE Transactions on Instrumentation and Measurement*, vol. 52, no. 1, 111-118, February 2003.
9. S. Peer, Zoughi, R., "Comparison of water and saltwater movement in mortar based on a semi empirical electromagnetic model," *Proc. of the 20th IEEE Instrumentation and Measurement Technology Conference*, vol. 1, 513-517, May 2003.
10. E. H. Weber, "Development and modeling of thermally conductive polymer/carbon composites", *Ph.D Dissertation*, Michigan Technological University, 2001.
11. S. V. Egorov, A. G. Ereemeev, I. V. Plotnikov, V. E. Semenov, A. A. Sorokin, N. A. Zharova and Y. V. Bykov, "Edge effect in microwave heating of conductive plates", *Journal Of Physics D: Applied Physics*, vol. 39, pp. 3036-3041, 2006.
12. C. Meola, and G. M. Carlomagno, "Recent advances in the use of infrared thermography", *Measurement Science and Technology*, vol. 15, pp.27-58, 2004.
13. DRS Thermal Camera, <http://www.drsinfrared.com>, accessed Feb. 2014.